Journal of Fluorine Chemistry 144 (2012) 1–6

Contents lists available at SciVerse ScienceDirect

Journal of Fluorine Chemistry

journal homepage: www.elsevier.com/locate/fluor

Interionic cross relaxation and tunable color luminescence in $KY_3F_{10}:Tb^{3+}$ nano/microcrystals synthesized by hydrothermal approach

Jinsu Zhang [a,*], Baojiu Chen [a,*], Zuoqiu Liang [a], Xiangping Li [a], Jiashi Sun [a], Ruixia Zhong [b], Lihong Cheng [a], Haiyang Zhong [a]

[a] Department of Physics, Dalian Maritime University, Dalian, Liaoning 116026, PR China
[b] Department of Materials Science and Engineering, Northeastern University at Qinhuangdao Branch, Qinhuangdao 066004, PR China

ARTICLE INFO

Article history:
Received 26 June 2012
Received in revised form 3 September 2012
Accepted 8 September 2012
Available online 14 September 2012

Keywords:
$KY_3F_{10}:Tb^{3+}$
Cross relaxation
Inokuti–Hirayama model

ABSTRACT

Color tunable phosphors of $KY_{3(1-x)}Tb_{3x}F_{10}$ ($KY_3F_{10}:xTb^{3+}$) were synthesized by the hydrothermal (HT) approach. The luminescence consists of a group of blue and green emission lines originating from $^5D_3 \rightarrow {}^7F_J$ and $^5D_4 \rightarrow {}^7F_J$ transitions of Tb^{3+}, respectively. The emitting color tunes from blue to green by gradually increasing Tb^{3+} concentrations, which is attributed to the enhanced $^5D_3$–$^5D_4$ cross-relaxation (CR) between two Tb^{3+} ions, as described by ($^5D_3$, $^7F_6$)–($^5D_4$, $^7F_0$). The CR process is analyzed based on Inokuti–Hirayama model and ascribed to the electric dipole–dipole interaction. The energy transfer critical distance and critical concentration between Tb^{3+} ions are evaluated to be 8.03 Å and 4.61×10^{20} cm^{-3}, respectively. Moreover, the initial transfer rate on acceptor concentration is also presented with an averaged CR coefficient.

1. Introduction

Rare earth ions doped fluoride phosphors have attracted extensive attention owing to their potential applications in lighting sources, displays, optical transmission, medical diagnostics, and biological fluorescence labels, etc. [1–4]. The fluoride material KY_3F_{10} with the cutoff phonon frequency of 400 cm^{-1} is applied as a laser material for the good optical and thermo-mechanical properties [5]. The complex fluorides are conventionally synthesized by crystal growth or solid-state reaction method [6–8]. However, such reaction requires high temperature, complicated setup and pure inert atmosphere to avoid contamination from oxygen. Recently, as a potential use in biolabels, the synthesis methods for fluorides have been rapidly developed [9,10]. The hydrothermal (HT) approach is proven to be a good choice to synthesize $KY_3F_{10}:Tb^{3+}$ phosphor with homogeneous and regular morphology due to the convenience, exemption from pollution, and the possibility of achieving satisfactory crystalline at a relatively low temperature.

Among rare earth ions doped materials, the Tb^{3+} doped phosphors exhibit efficient green-emitting and have been used in the display and lighting fields, such as $Y_2O_2S:Tb^{3+}$ used in color television, $LaPO_4:Ce^{3+}$, Tb^{3+} used in plasma display panel (PDP) and $LaMgAl_{11}O_{19}:Ce^{3+}$, Tb^{3+} used in the fluorescent lamp. The green-emitting lines are originating from the $^5D_4$ energy-level. In some cases, Tb^{3+} ions can also emit blue-sharp emission lines originating from the energy-level of $^5D_3$. The non-radiative energy transfer from $^5D_3$ to $^5D_4$ plays an important role in the luminescence of Tb^{3+} doped phosphors. The quantitative theories for the non-radiative energy transfers have been given by Förster [11] and Dexter [12,13]. Furthermore, many efforts have been made to establish the theoretical model for describing the interionic interaction [14–20]. Lots of research concerning the energy transfer in solids has been carried out in order to develop novel luminescent materials for white light emitting diode, long lasting phosphors and so on [21–24].

In this paper, the $KY_3F_{10}:Tb^{3+}$ nano/microcrystals were synthesized by hydrothermal approach. We observed tunable color luminescence in Tb^{3+} doped KY_3F_{10} as a function of Tb^{3+} concentrations after UV excitation. The blue and green emissions were detected, and with increasing Tb^{3+} concentrations, the color was tuned from blue to green, which was attributed to the CR between Tb^{3+} ions, as described by ($^5D_3$, $^7F_6$)–($^5D_4$, $^7F_0$). The interionic CR process in $KY_3F_{10}:Tb^{3+}$ was studied. The electric multipole interaction was identified for the cross relaxation between Tb^{3+}. The energy transfer critical distance and critical concentration between the Tb^{3+} ions were evaluated based on the Inokuti–Hirayama model.

* Corresponding authors. Tel.: +86 411 8472 8909; fax: +86 411 8472 8909.
E-mail addresses: zhangjinsu@gmail.com (J. Zhang), baojiuchen@gmail.com (B. Chen).

0022-1139/$ – see front matter © 2012 Elsevier B.V. All rights reserved.
http://dx.doi.org/10.1016/j.jfluchem.2012.09.003

2. Results and discussion

2.1. Structural and morphology characteristics

The crystalline structure of the KY_3F_{10} samples A and B doped with 1 mol% Tb^{3+} was investigated by the XRD. The rare-earth compound of KY_3F_{10} has a face centered cubic structure. The space group is $Fm\bar{3}m(O_h^5)$ and the symmetry of the rare earth sites is tetragonal C_{4v}, with the fourfold symmetry axis oriented along one of the three cubic axes. The XRD data were collected by using a scanning mode in the 2θ ranging from 20° to 70° as shown in Fig. 1. Both the sample A and B can be indexed to the pure KY_3F_{10} phase based on the standard card (JCPDS no. 27-0465) as shown at the bottom of Fig. 1. It can be found that the XRD peaks are broad for the sample A, reflecting the smaller particle size as is identified with the FE-SEM image shown in the top-right corner of Fig. 1. The particle size distribution is in the range from 20 to 40 nm. The XRD peaks for the sample B are accurately accordant with the standard card. Another inserted FE-SEM image shows morphology for the sample B. It can be seen that the particle size of sample B became much larger after thermal treatment in comparison with the as prepared one. The average particle size is several hundreds nanometers.

2.2. Luminescence characteristics

Fig. 2 shows the excitation (λ_{em} = 414 nm) and emission (λ_{ex} = 218 nm) spectra of KY_3F_{10}:0.01Tb^{3+} (solid lines). The excitation spectrum by monitoring the 414 nm emission is composed of an intense broad band responsible for the $^7F_6 \rightarrow 4f^7 5d$ transition and some weak lines corresponding to the f-f transitions of Tb^{3+}. Upon the $4f^7 5d$ excitation at 218 nm, there appear two groups of emissions. The blue emission lines peaking at 382, 414, 436, 456 and 468 nm originate from the $^5D_3 \rightarrow {}^7F_J$ transitions, and the green emission lines peaking at 488, 542, 584 and 622 nm come from the $^5D_4 \rightarrow {}^7F_J$ transitions, respectively. The energy of $^5D_3$ is about 5800 cm^{-1} higher than that of $^5D_4$. The de-excitation from $^5D_3$ to $^5D_4$ is owing to cross-relaxation (CR) and multi-phonon relaxation processes. The CR process depends on the Tb^{3+} concentration, and the multi-phonon relaxation process is related to the phonon frequency of the host. For a four- to five-phonon process, radiative and nonradiative decay have comparable probabilities. However, if the band gap requires six or more phonons to bridge it, the nonradiative relaxation becomes too slow to compete. Therefore, Tb^{3+} activated phosphors with tunable emitting colors can be achieved by choosing a low phonon frequency host. We summarize the reported tunable color luminescence in Tb^{3+} doped materials [25–41], as shown in Table 1. The approximate values of the phonon frequency in some oxides containing ionic complexes and fluoride compounds have been reported, such as borates (~1300 cm^{-1}), phosphates (~1200 cm^{-1}), silicates (~1050 cm^{-1}), tungstates (~900 cm^{-1}), aluminates (~850 cm^{-1}), fluorides (~450 cm^{-1}). It is found that if the phonon frequency of the host is low enough (~1000 cm^{-1}), the emission from $^5D_3$ will be detected due to the invalid multiphonon relaxation. The low phonon frequency is needed to achieve the tunable blue-green phosphor. We can see that the phonon frequency in fluorides is lower than that in oxides containing ionic complexes. Though it is higher than that in chlorides and bromides, the fluorides are more chemical stability than other halides. Moreover, the elements Tb and Y belong to the same group, which is propitious for Tb^{3+} to dope in KY_3F_{10}. Fig. 3 shows the PL spectra of KY_3F_{10}:Tb^{3+} with different Tb^{3+} concentrations under 218 nm excitation, where the intensities of the blue

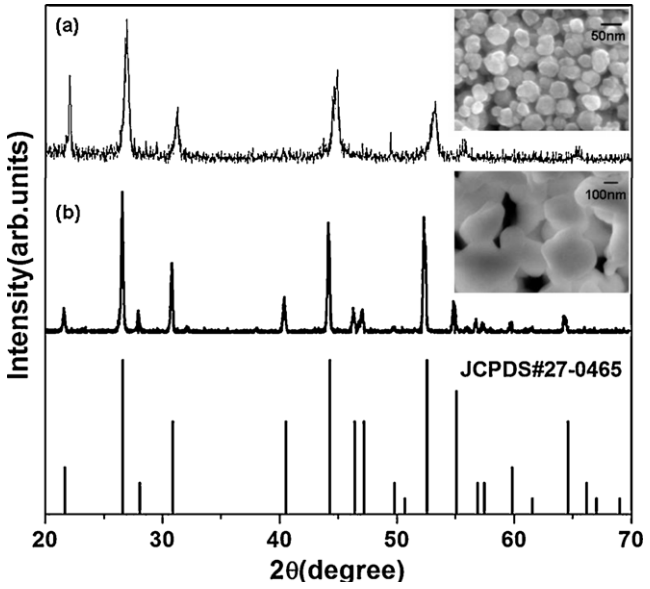

Fig. 1. XRD patterns of KY_3F_{10}:0.01Tb^{3+} sample A (a), sample B (b) and the standard KY_3F_{10} pattern (JCPDS #27-0465) (inset: SEM patterns for the same samples).

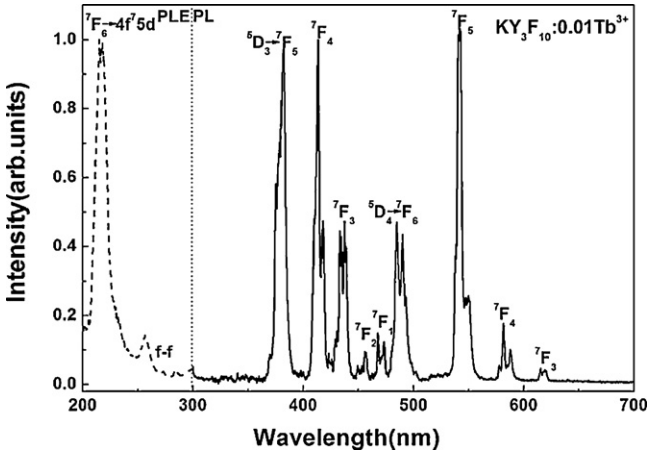

Fig. 2. PLE (λ_{em} = 414 nm) and PL (λ_{ex} = 218 nm) spectra of KY_3F_{10}:0.01Tb^{3+}(solid lines) and phosphorescence emission spectrum of KY_3F_{10}:0.01Tb^{3+}(dashed line).

Table 1
Blue-green tunable color luminescence in Tb^{3+}-doped oxides containing ionic complexes and halide compounds.

	Host [ref.]
Oxides containing ionic complexes	$Y_4Al_2O_9$ [25]
	$Li_4SrCa(SiO_4)_2$ [26]
	$CaWO_4$ [27]
	$CaSc_2O_4$ [28]
	$Li(Y, Gd)(PO_3)_4$ [29]
	$LaGaO_3$ [30]
	$CsYP_2O_7$ [31]
	$Y_3Al_5O_{12}$ [32]
	$GdTaO_4$ [33]
Halide compounds	$Ca_6Ln_2Na_2(PO_4)_6F_2$ (Ln = Gd, La) [34]
	Rb_2KInF_6 [35]
	β-$NaYF_4$ [36]
	K_2YF_5 [37]
	ZBLAN [38]
	α-GdOF [39]
	$CsMgCl_3$ [40]
	$CsMgBr_3$ [40]
	$CsCdBr_3$ [40,41]

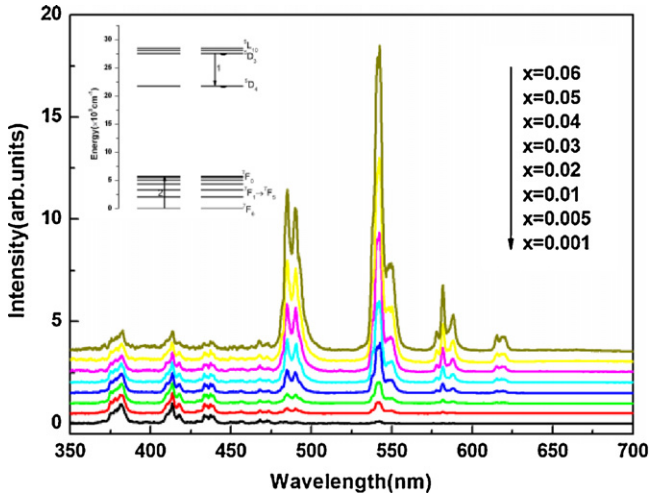

Fig. 3. PL spectra of KY_3F_{10}:xTb^{3+} recorded after 218 nm excitation, where the intensities of the blue emission originating from $^5D_3$ are normalized (inset: schematic energy levels of KY_3F_{10}:Tb^{3+} showing physical mechanisms for cross-relaxation energy transfer).

emission originating from $^5D_3$ are normalized. At low concentrations of Tb^{3+}, the blue emissions from the $^5D_3$ level are dominant in the fluorescence spectra, indicating that the $^5D_3$ level is effectively populated when excited at 4f^{7}5d configuration. The emission intensity ratio of green to blue enhances remarkably with increasing Tb^{3+} concentration, which is attributed to the enhancement of the cross relaxation energy transfer among Tb^{3+} ions as shown in the inset of Fig. 3. A donor Tb^{3+} ion decays nonradiatively from the excited state $^5D_3$ to the $^5D_4$, simultaneously, a nearby acceptor Tb^{3+} ion is excited from its ground state $^7F_6$ to an intermediate state $^7F_0$, then the Tb^{3+} ion at $^7F_0$ returns to ground state via multiphonon relaxation. It can be sure that the change in profile of the emission spectrum would cause a variation of the color coordinates of KY_3F_{10}:Tb^{3+} phosphor. Fig. 4 shows dependence of color coordinates on the Tb^{3+} doping concentration in the Commission on Illumination

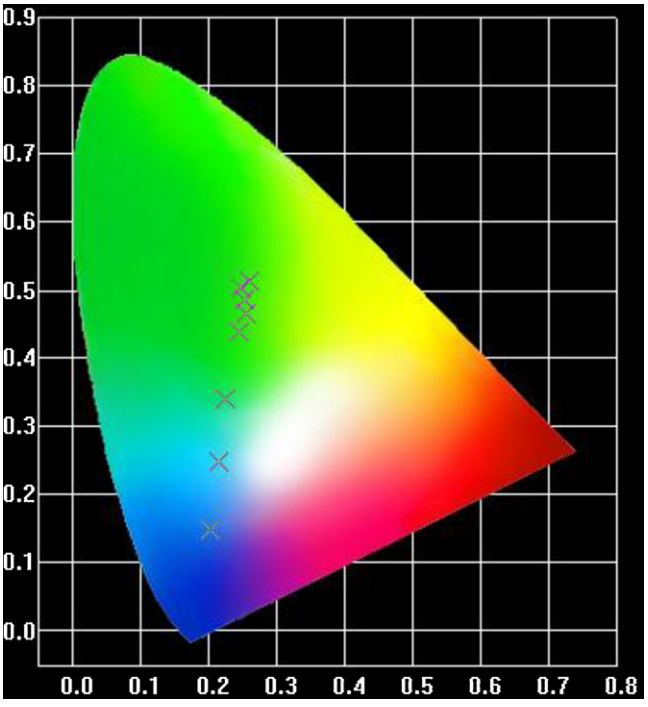

Fig. 4. CIE chromaticity diagram according to the PL spectra.

(CIE) chromaticity diagram. It is seen that the color coordinates of KY_3F_{10}:Tb^{3+} phosphor can be tuned in a large extent from blue to green by increasing the Tb^{3+} doping concentration.

2.3. CR energy transfer

In principle, the mechanism for energy transfer between luminescent centers can be classified as dipole–dipole (D–D) interaction, dipole–quadrupole (D–Q) interaction, quadrupole–quadrupole (Q–Q) interaction, and exchange interaction [12]. For exchange interaction, the energy transfer rate depends strongly on the donor–acceptor distance R which is much shorter than that for electric multipolar interaction. In general, the exchange interaction will dominate when the critical distance R_0 is shorter than 3–4 Å [22]. In this work, the average distance between Tb^{3+} ions is estimated by [12,19]:

$$R_{\mathrm{Tb}} = \left[\frac{3}{4\pi n_A}\right]^{1/3} \tag{1}$$

where n_A is given by xN_Y with $N_Y = n/V$ being the number of Y sites per unit volume in KY_3F_{10}. x is the Tb^{3+} doping concentration, n is the number of lattice sites that can be occupied by Y^{3+} ions in a unit cell, and V is the volume of the crystallographic unit cell. In our present case, $V = 1542$ Å^3 and $n = 24$, $N_Y = 1.56 \times 10^{22}$ cm^{-3}. The calculated values of R_{Tb} are 24.8, 14.5, 11.6, 9.2, 8.0, 7.3, 6.8 and 6.4 Å when the Tb^{3+} doping concentration (the molar ratio of Tb^{3+} to Y^{3+}) equals 0.001, 0.005, 0.01, 0.02, 0.03, 0.04, 0.05 and 0.06, respectively. Thus, it can be concluded that the cross relaxation between Tb^{3+} may occur via the electric multipole interaction.

The enhancement of CR can decrease the lifetime of the $^5D_3$ level, while the lifetime of the $^5D_4$ level is unaffected if the Tb^{3+} concentration is below the quenching point [12]. In order to analyze the dynamic process of the CR, the fluorescence lifetimes of $^5D_3(\tau)$ for samples with different Tb^{3+} concentrations were measured upon 355 nm pulsed laser excitation as represented in Fig. 5. The decay of $^5D_3$ remains exponential function for the sample of KY_3F_{10}:0.001Tb^{3+}, and with the increasing of Tb^{3+}concentration, it becomes non-exponential function. The mean lifetimes are calculated according to the Inokuti–Hirayama model as following definition [12]:

$$\langle\tau\rangle = \frac{\int_0^\infty I(t)t\,dt}{\int_0^\infty I(t)\,dt} \tag{2}$$

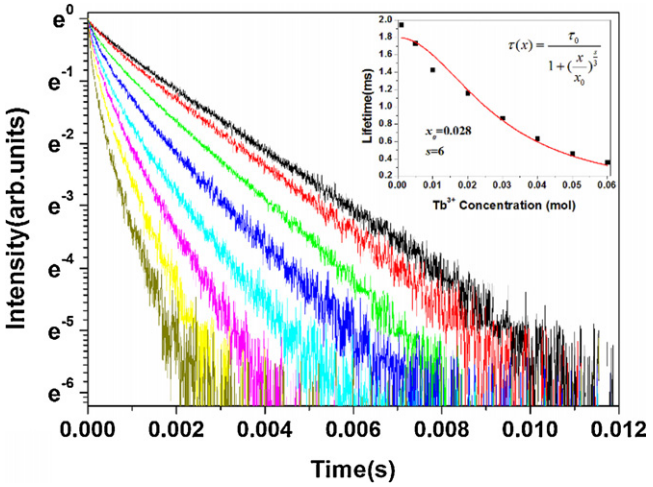

Fig. 5. Fluorescence lifetimes of $^5D_3$ of KY_3F_{10}:xTb^{3+} (inset: dependence of fluorescent lifetime of $^5D_3$ on Tb^{3+} doping concentration, solid curve is the fitting curve derived based on the Dexter's model).

where $I(t)$ represents the fluorescent intensity at time t. The values are 1.95, 1.73, 1.42, 1.16, 0.87, 0.63, 0.46 and 0.36 ms and represented in the inset of Fig. 5. The experimental data are well fitted with the relationship established by Dexter [12]:

$$\tau(x) = \frac{\tau_0}{1 + (x/x_0)^{s/3}} \tag{3}$$

where τ_0 is the intrinsic decay lifetime of the donor (Tb^{3+}), $\tau(x)$ is fluorescent lifetime at accepter (Tb^{3+}) concentration x, x_0 is the critical concentration with the same dimension as the doping concentration x, and s = 6, 8 or 10, indicating D–D, D–Q and Q–Q interactions, respectively. It was found from the fitting process that s is close to 6, thus implying that the possible energy transfer mechanism is D–D. For the slightly doped sample of KY_3F_{10}:0.001Tb^{3+}, the CR energy transfer from $^5D_3$ to $^5D_4$ is negligible, and the multi-phonon relaxation is considered to be the only way to make the $^5D_4$ populated. The decay time 1.95 ms of $^5D_3$ in KY_3F_{10}:0.001Tb^{3+} obtained from a pure exponential decay is assumed as the initial lifetime of $^5D_3$(τ_0). In the present system, the critical concentration x_0 is fitted to be 0.028 mol. Therefore, the average distance between Tb^{3+} can be calculated to be 8.17 Å by Eq. (1), which is considered as the critical distance for the Tb^{3+} in KY_3F_{10}.

In the above analysis, we present an intuitive method to determine the ionic interaction. The critical concentration and distance are approximated. For a donor–acceptor system, the fluorescence decay curves in Fig. 5 reflect the dynamic process of energy transfer. It can be seen that the decay curve of $^5D_3$ for the sample of KY_3F_{10}:0.001Tb^{3+} remains exponential function and can be described as

$$I_{D0}(t) = I_0 \exp\left(-\frac{t}{\tau_0}\right) \tag{4}$$

where $I_{D0}(t)$ is the luminescence intensity at time t, I_0 is the luminescence intensity at t = 0 and τ_0 is the intrinsic lifetime of $^5D_3$. With increasing Tb^{3+} doping concentration, the decay curves become non-exponential. It is well known that the Inokuti–Hirayama (I–H) model has succeeded in describing the non-exponential fluorescent decay, in which the intensity can be expressed as follows [14]:

$$I_D(t) = I_0 \exp\left[-\frac{t}{\tau_0} - \frac{4}{3}\pi\Gamma\left(1-\frac{3}{s}\right)n_A R_0^3\left(\frac{t}{\tau_0}\right)^{3/s}\right] \tag{5}$$

where $I_D(t)$ is the fluorescent intensity at time t for the system in the presence of energy transfer. s = 6, 8, and 10, are for D–D, D–Q, and Q–Q interactions, respectively. $\Gamma(1-3/s)$ is a Gamma function, n_A is the number of acceptor ions per unit volume, and R_0 is the critical distance. According to Eqs. (4) and (5), we can obtain that

$$\frac{I_D(t)}{I_{D0}(t)} = \exp\left[-\frac{4}{3}\pi\Gamma\left(1-\frac{3}{s}\right)n_A R_0^3\left(\frac{t}{\tau_0}\right)^{3/s}\right] \tag{6}$$

The ratio $I_D(t)/I_{D0}(t)$ characterizes the decay of excited donors to the acceptors via CR. From Eq. (6), one has

$$\ln\left[\frac{I_D(t)}{I_{D0}(t)}\right] = -\frac{4}{3}\pi\Gamma\left(1-\frac{3}{s}\right)n_A R_0^3\left(\frac{1}{\tau_0}\right)^{3/s}(t)^{3/s} \tag{7}$$

and

$$\log_{10}\left\{\ln\left[\frac{I_D(t)}{I_{D0}(t)}\right]\right\} = \log_{10}\left[-\frac{4}{3}\pi\Gamma\left(1-\frac{3}{s}\right)n_A R_0^3\left(\frac{1}{\tau_0}\right)^{3/s}\right] + \frac{3}{s}\log_{10} t \tag{8}$$

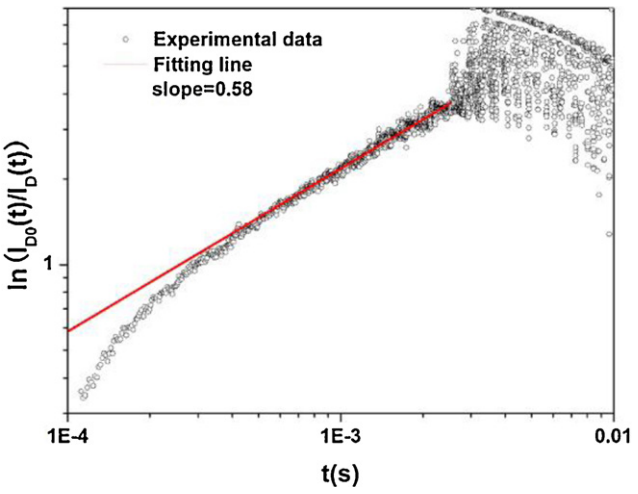

Fig. 6. The relationship of $\ln(I_{D0}(t)/I_D(t))$ vs t plotted in a double logarithmic coordinate for sample KY_3F_{10}:$x$$Tb^{3+}$ with x = 0.01.

According to Eq. (8), $\log_{10}\{\ln[I_{D0}(t)/I_D(t)]\}$ acts as a linear function of $\log_{10} t$ with a slope of $3/s$. Fig. 6 shows the log–log plot of $\ln[I_D(t)/I_{D0}(t)]$ versus t for sample 0.01 Tb^{3+} doped KY_3F_{10}. It is demonstrated that the slope for $t > 0.5$ ms is 0.58 which is more close to 1/2, indicating an electric dipole–dipole interaction for CR. From Eq. (7), $\ln[I_D(t)/I_{D0}(t)]$ is proportional to $t^{s/3}$ with a slope of $-(4/3)\pi\Gamma(1-3/s)n_A R_0^3(1/\tau_0)^{3/s}$. Regarding s as 6, we have plotted $\ln[I_D(t)/I_{D0}(t)]$ versus $t^{1/2}$ for the samples KY_3F_{10}:$x$$Tb^{3+}$ with x = 0.005, 0.01, 0.02, 0.03, 0.04, 0.05 and 0.06 mol, as shown in Fig. 7. The best fitting to the curves of Tb^{3+} concentration in range from 0.005 to 0.04 mol yields the value $R_0^6/\tau_0 = 1.38 \times 10^{-40}$ cm^6 s^{-1}, where $1/\tau_0$ is the CR rate between the donor and acceptor at the critical distance with τ_0 = 1.94 ms, then R_0 is calculated to be 8.03 Å. The critical concentration can be determined by $n_0 = 3/4\pi R_0^3$, receiving a value of 4.61×10^{20} cm^{-3}, which denotes the Tb^{3+} doping concentration x = 0.03 mol. The critical concentration calculated by I–H model has a good match with the value derived from Eq. (3) through a numeric fitting. Fig. 7 shows large deviation between the experimental data and fitting curves for the samples KY_3F_{10}:$x$$Tb^{3+}$ with x = 0.05 and 0.06 mol, which suggests that the I–H model is not available. The I-H model is applicable with a precondition that the energy migration between the donors can be neglected. In the present system, the critical concentration is around 0.03 mol. With the

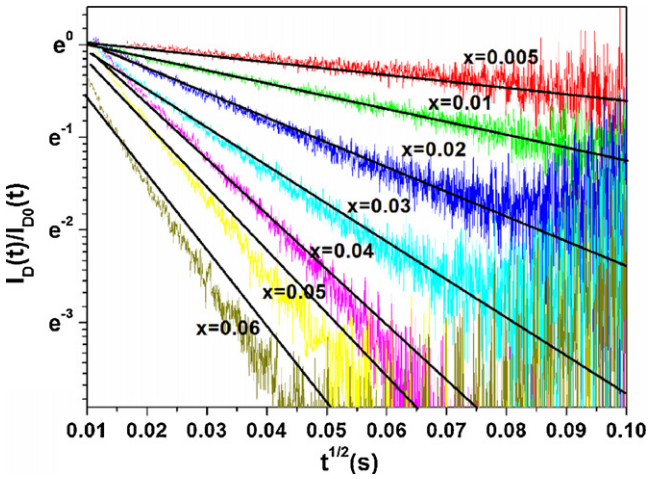

Fig. 7. $\ln(I_D(t)/I_{D0}(t))$ vs $t^{1/2}$ for the samples KY_3F_{10}:$x$$Tb^{3+}$, the solid lines indicate the fitting results.

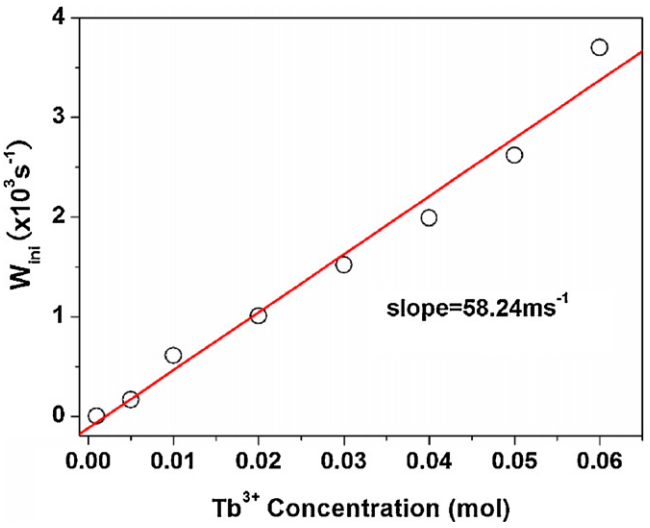

Fig. 8. The initial energy transfer rates of $^5D_3$ to $^5D_4$ as a function of Tb^{3+} concentrations.

doping concentration increases, the energy migration between donors may get faster. This fast energy migration effectively averages over the various individual donor environments so that the CR rate is the same for all donors and can be written as $W_{CR} = \langle W_q \rangle x$ [17]. Moreover, Eq. (5) is not applicable at initial times, because it is obtained by assuming the nearest distance between a donor and an acceptor to be 0, leading to an infinite initial CR rate. Fig. 6 shows an increase in slope when the time t is below 0.5 ms, which exhibits that Eq. (5) is not applicable. The increase in slope (when t is below 0.5 ms) exhibits linear behavior $f(t) = \exp(-W_{ini}t)$ compared with a $t^{3/s}$ variation at longer times. The energy transfer rate can be described by $W_{ini} = \langle \tau_D \rangle_{ini}^{-1} - \langle \tau_0 \rangle^{-1}$ with $\langle \tau_D \rangle_{ini}^{-1}$ is the initial decay rate. Fig. 8 shows a linear dependence of W_{ini} on x. The slope gives a constant around 58.24 ms^{-1}.

3. Conclusions

The Tb^{3+} doped KY_3F_{10} phosphors have been prepared by the hydrothermal approach, which exhibit two groups of emissions originating from $^5D_3$ and $^5D_4$ energy-levels. The intensity ratio of blue to green-emitting is reduced with increasing Tb^{3+} concentrations via the CR described by ($^5D_3$, $^7F_6$)–($^5D_4$, $^7F_0$). According to the I-H model, the electronic dipole–dipole interaction between Tb^{3+} governs the dynamic CR process. The CR parameters are determined with the critical CR distance $R_0 = 8.03$ Å and the critical concentration $n_0 = 4.61 \times 10^{20}$ cm^{-3}. Moreover, we also discuss the status of the initial decay curves which the I–H model is not available. The dependence of averaged CR rate on acceptor concentration is presented with a CR coefficient to be 58.24 ms^{-1}.

4. Experimental

4.1. Sample preparation

Aqueous solutions of kalium fluoride (KF, AR grade) and ammonium hydrogen fluoride (NH_4HF_2, AR grade) with a molar ratio of 1.0/4.5 were mixed in a Teflon beaker to form a clear solution 1. Another mixed solution 2 of $Ln(NO_3)_3$ (here $Ln^{3+} = Y^{3+}$ and Tb^{3+}, and the molar ratios of Tb^{3+} to Y^{3+} are 0.001, 0.005, 0.01, 0.02, 0.03, 0.04, 0.05, 0.06) and ethylenediamine tetraacetic acid (EDTA) with a molar ratio of 1.0/1.0 was prepared in a Teflon cup. A milky suspension was first formed when the clear solution 1 was added into solution 2 with a molar ratio of 20/3 under stirring for 1 h. The initial pH value of the reaction system was around 3.0. The suspension was then filled in a Teflon-lined stainless steel autoclave and sealed for hydrothermal crystallization at 170 °C for 18 h. After the autoclaves were cooled, the white powder (sample A) were washed with distilled water and dried in a desiccator at 80 °C, then annealed at 300 °C for 2 h to get the final product (sample B).

4.2. Characterization

The crystalline structures were characterized by X-ray diffraction (XRD) (Rigaku D/max-rA power diffractometer with Cu KR (λ = 1.54178 Å) radiation source). Field emission scanning electron microscopy (FE-SEM) (Hitachi S-4800, Japan) was used to determine the morphology of the studied samples. Photoluminescence (PL) and photoluminescence excitation (PLE) spectra of the phosphors were measured by using HITACHI F-4600 fluorescence spectrophotometer. In fluorescence lifetime measurements, the third (355 nm) harmonic of a Nd-YAG laser (Spectra-Physics, GCR 130) was used as excitation source, and the signal was detected with a Tektronix digital oscilloscope model (TDS 3052). All of the above measurements were performed at room temperature.

Acknowledgements

This work is financially supported by the National Natural Science Foundation of China (Grant nos. 11104024, 50972021, 61078061 and 11104023), Scientific Research Fund for Doctoral Program of Liaoning Province (Grant nos. 20111031 and 20111032), Foundation of Education Department of Liaoning Province (Grant no. L2010057), Fundamental Research Funds for the Central Universities (Grant nos. 2011JC036, 2012TD017, 2011QN152) and the Major Research Plan of the Natural Science Foundation of Hebei Province, China (Grant no. A2010001379).

References

[1] L.Y. Wang, R.X. Yan, Z.Y. Huo, L. Wang, J.H. Zeng, J. Bao, X. Wang, Q. Peng, Y.D. Li, Angewandte Chemie International Edition 2044 (2005) 6054–6057.
[2] F.T. You, S.H. Huang, S.M. Liu, Y. Tao, Journal of Solid State Chemistry 177 (2004) 2777–2782.
[3] J.C. Boyer, F. Vetrone, L.A. Cuccia, J.A. Capobianco, Journal of the American Chemical Society 128 (2006) 7444–7445.
[4] A.F.H. Librantza, L. Gomesa, S.L. Baldochia, I.M. Ranieria, G.E. Brito, Journal of Luminescence 121 (2006) 137–148.
[5] P. Porcher, P. Caro, Journal of Chemical Physics 65 (1976) 89–94.
[6] A. Yoshikawa, K. Kamada, M. Nikl, K. Aoki, H. Sato, J. Pejchal, T. Fukuda, Journal of Crystal Growth 285 (2005) 445–449.
[7] M. Karbowiak, A. Mech, L. Kępiński, W. Mielcarek, S. Hubert, Journal of Alloys and Compounds 400 (2005) 67–75.
[8] J.S. Zhang, Z.D. Hao, X. Zhang, Y.S. Luo, X.G. Ren, X.J. Wang, J.H. Zhang, Journal of Applied Physics 106 (2009) 034915.
[9] J. Shen, L.D. Sun, Y.W. Zhang, C.H. Yan, Chemical Communications 46 (2010) 5731–5733.
[10] C. Chao, W. Qin, J. Zhang, Y. Wang, P. Zhu, G. Wang, G. Wei, L. Wang, L. Jin, Journal of Fluorine Chemistry 129 (2008) 204–209.
[11] T. Förster, Z. Naturforsch. 4a (1949) 321.
[12] D.L. Dexter, James H. Schulman, Journal of Chemical Physics 22 (1954) 1063–1070.
[13] D.L. Dexter, C.C. Klick, G.A. Russell, Physical Review 100 (1955) 603–605.
[14] M. Inokuti, F. Hirayama, Journal of Chemical Physics 43 (1965) 1978–1989.
[15] G. Blasse, Physics Letters 28A (1968) 444–445.
[16] P.M. Selzel, D.L. Huber, B.B. Bamett, Y.M. Yen, Physical Review B 17 (1978) 4979–4995.
[17] B. Büchner, M. Breuer, A. Freimuth, A.P. Kampf, Physical Review Letters 73 (1994) 1841–1844.
[18] G. Blasse, A. Bril, Journal of Chemical Physics 47 (1967) 1920–1926.
[19] W. Lenth, G. Huber, D. Fay, Physical Review B 23 (1981) 3877–3885.
[20] C. Andraud, J.P. Denis, B. Blanzat, A. Vedrine, Chemical Physics Letters 101 (1983) 357–360.
[21] L. Wang, X. Zhang, Z.D. Hao, Y.S. Luo, J.H. Zhang, X.J. Wang, Journal of Applied Physics 108 (2010) 093515.
[22] J. Yang, C.M. Zhang, C.X. Li, Y.N. Yu, J. Lin, Inorganic Chemistry 47 (2008) 7262–7270.

[23] J.H. Zhang, L. Wang, Y. Jin, X. Zhang, Z.D. Hao, X.J. Wang, Journal of Luminescence 131 (2011) 429–432.
[24] H. Jiao, F.H. Liao, S.J. Tian, X.P. Jing, Journal of the Electrochemical Society 150 (2003) H220–H224.
[25] Z. Boruc, B. Fetlinski, M. Kaczkan, S. Turczynski, D. Pawlak, M. Malinowski, Journal of Alloys and Compounds 532 (2012) 92–97.
[26] X.M. Zhang, H.J. Seo, Materials Research Bulletin 47 (2012) 2012–2015.
[27] Y. Tian, B.J. Chen, H.Q. Yu, R.N. Hua, X.P. Li, J.S. Sun, L.H. Cheng, H.Y. Zhong, J.S. Zhang, Y.F. Zheng, T.T. Yu, L.B. Huang, Journal of Colloid and Interface Science 360 (2011) 586–592.
[28] Z.D. Hao, J.H. Zhang, X. Zhang, S.Z. Lu, X.J. Wang, Journal of the Electrochemical Society 156 (2009) H193–H196.
[29] B. Han, H.B. Liang, Y. Huang, Y. Tao, Q. Su, Journal of Physical Chemistry C 114 (2010) 6770–6777.
[30] X.M. Liu, R. Pang, Z.W. Quan, J. Yang, J. Lin, Journal of the Electrochemical Society 154 (2007) J185–J189.
[31] A. Akrim, D. Zambon, J.C. Cousseins, Journal of Alloys and Compounds 207–208 (1994) 99–101.
[32] N. Bodenschatz, R. Wannemacher, J. Heber, D. Mateika, Journal of Luminescence 47 (1990) 159–167.
[33] M.J.J. Lammers, G. Blasse, Materials Research Bulletin 19 (1984) 759–768.
[34] M.B. Xie, Y. Tao, Y. Huang, H.B. Liang, Q. Su, Inorganic Chemistry 49 (2010) 11317–11324.
[35] M.A. Buñuel, L. Lozano, J.P. Chaminade, B. Moine, B. Jacquier, Optical Materials 13 (1999) 211–223.
[36] D. Zakaria, R. Mahiou, D. Avignant, M.H. Kettani, J.C. Cousseins, M. Zahir, Annales de Chimie Science des Matériaux 23 (1998) 263–266.
[37] P. Boutinaud, R. Mahiou, J.C. Cousseins, Journal of Luminescence 72–74 (1997) 318–320.
[38] A.M.A. van Dongen, Journal of Non-Crystalline Solids 139 (1992) 271–273.
[39] P.A.M. Berdowski, M.J.J. Lammers, G. Blasse, Chemical Physics Letters 113 (1985) 387–390.
[40] T.A. Lawrence, K.A. Murra, P.S. May, Journal of Physical Chemistry B 107 (2003) 4002–4011.
[41] P.S. May, K.D. Sommer, Journal of Physical Chemistry A 101 (1997) 9571–9577.